

A Monte Carlo Model Reveals Independent Signaling at Central Glutamatergic Synapses

Kevin M. Franks,*[†] Thomas M. Bartol, Jr.,* and Terrence J. Sejnowski*[†]

*Howard Hughes Medical Institute, Computational Neurobiology Laboratory, The Salk Institute for Biological Studies, La Jolla, California 92037; and [†]Division of Biology, University of California, San Diego, La Jolla, California 92093 USA

ABSTRACT We have developed a biophysically realistic model of receptor activation at an idealized central glutamatergic synapse that uses Monte Carlo techniques to simulate the stochastic nature of transmission following release of a single synaptic vesicle. For the a synapse with 80 AMPA and 20 NMDA receptors, a single quantum, with 3000 glutamate molecules, opened approximately 3 NMDARs and 20 AMPARs. The number of open receptors varied directly with the total number of receptors, and the fraction of open receptors did not depend on the ratio of co-localized AMPARs and NMDARs. Variability decreased with increases in either total receptor number or quantal size, and differences between the variability of AMPAR and NMDAR responses were due solely to unequal numbers of receptors at the synapse. Despite NMDARs having a much higher affinity for glutamate than AMPARs, quantal release resulted in similar occupancy levels in both receptor types. Receptor activation increased with number of transmitter molecules released or total receptor number, whereas occupancy levels were only dependent on quantal size. Tortuous diffusion spaces reduced the extent of spillover and the activation of extrasynaptic receptors. These results support the conclusion that signaling is spatially independent within and between central glutamatergic synapses.

INTRODUCTION

Fast excitatory signaling in the central nervous system occurs when a synaptic vesicle fuses with the presynaptic membrane, allowing glutamate to diffuse across the synaptic cleft and bind to postsynaptic ionotropic receptors, including α -amino-3-hydroxy-5-methyl-isoxazolepropionic acid receptors (AMPA) and *N*-methyl-D-aspartate receptors (NMDARs). AMPAR and NMDAR receptors are co-localized at many glutamatergic synapses (Bekkers and Stevens, 1989; Kharazia et al., 1996; Kharazia and Weinberg, 1999; Takumi et al., 1999; McAllister and Stevens, 2000; Racca et al., 2000), most of which are found on dendritic spines (Harris and Kater, 1994). The number of AMPARs found at individual synapses is highly variable, and appears to scale with the synaptic area (Nusser et al., 1998; Takumi et al., 1999; Kharazia and Weinberg, 1999; Racca et al., 2000). Interestingly, larger synapses are more potent than smaller ones (Matsuzaki et al., 2001), and synaptic responses elicited from distal sites on CA1 pyramidal cells generate larger postsynaptic currents (EPSCs) (Magee and Cook, 2000) and contain more receptors (Andrasfalvy and Magee, 2001) than proximal sites (but see Williams and Stuart, 2002). In addition, the dynamic regulation of AMPAR number at individual synapses is suggested to underly the long-term synaptic plasticity (Liao et al., 1995; Isaac et al., 1995; Shi et al., 1999; Carroll et al., 1999; Hayashi et al.,

2000). This assumes that bigger synapses contain more receptors and synapse potency scales with receptor number.

However, several fundamental issues remain unresolved. For example, how does increasing receptor number increase synapse potency? The number of receptors opened following quantal release may vary directly with the total number of receptors at the synapse, but other, more complex, interactions may occur. Because the number of glutamate molecules released in a quantum is finite, competition for transmitter may reduce potency when a large number of receptors are present. Alternatively, more receptors, particularly high-affinity NMDARs (Patneau and Mayer, 1990) may slow transmitter clearance from the cleft, transiently trapping transmitter near other receptors, and thus potentiate the AMPA response. What fraction of receptors are saturated following the release of a single quantum, and is a larger synapse, with more receptors less saturated than a smaller one? Direct measurements of these parameters at a single synapse in a complex neuropil are extremely difficult, and many perturbations at the synapse are experimentally impossible, motivating a biophysically realistic model of receptor activation at a single synapse.

We have therefore developed a model of an idealized central excitatory synapse using Monte Carlo methods. We examine the time course of synaptic glutamate concentrations following instantaneous release and rapid diffusion out of the cleft, the activation and time course of synaptic receptors following quantal release, and examine the dependence of receptor activation and occupancy levels on the quantal size (q) and the total number of receptors at the synapse (n). We also explore the spatial extent of glutamate diffusion out of the synapse and the conditions under which we are able to activate receptors at a neighboring synapse in either a simple or a tortuous geometry. The model makes

Submitted August 30, 2001, and accepted for publication June 4, 2002.

Address reprint requests to Terrence J. Sejnowski, Computational Neurobiology Laboratory, The Salk Institute, 10010 North Torrey Pines Road, La Jolla, CA 92037. Tel: 858-453-4100 x1611; Fax: 858-587-0417; E-mail: terry@salk.edu.

© 2002 by the Biophysical Society

0006-3495/02/11/2333/16 \$2.00

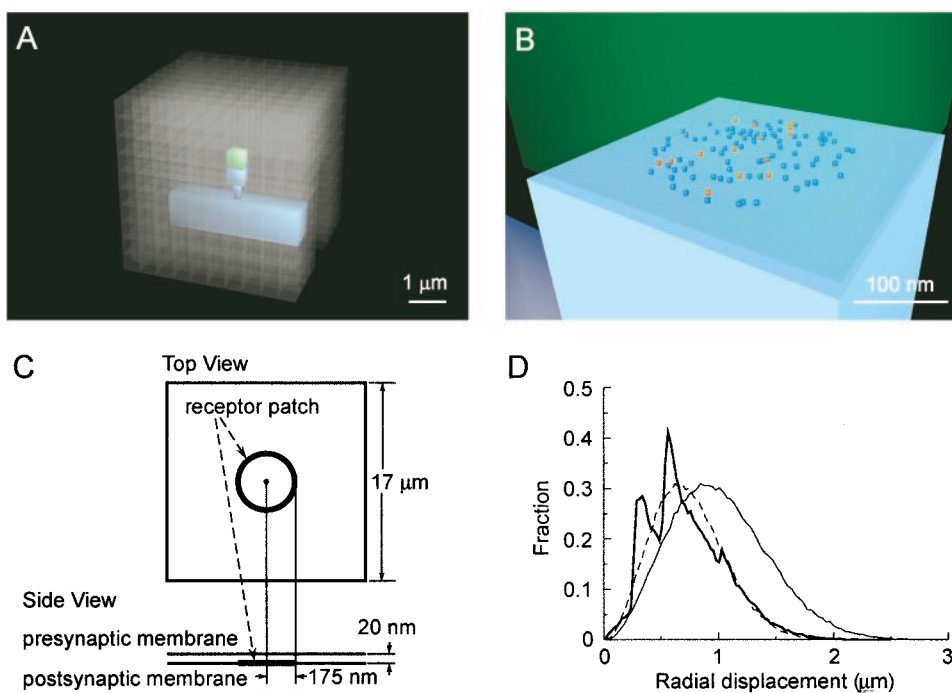


FIGURE 1 Representation of geometric structure of surfaces. (A) Embedded within a neuropil composed of cuboidal elements was a segment of dendrite containing a spine, attached to the dendritic shaft by a thin neck, and a presynaptic bouton. (B) The presynaptic bouton and synaptic face of the spine were separated by a 20-nm synaptic cleft. AMPA (blue) and NMDA (red) receptors were uniformly distributed across the surface of PSD on the spine. (C) Simple neural volume (sheet) consisted of two flat sheets separated by 20 nm, with AMPAR and NMDARs located on a central disk (not to scale). (D) Distribution of molecules after 1 ms of free diffusion (*thin trace*) and diffusion in the neuropil (*thick trace*). Tortuosity $(D/D_{app})^{1/2}$ of the neuropil was calculated by scaling the neuropilar distribution of ligand to match the free diffusion distribution (*dashed trace*).

quantitative predictions of the magnitude or time courses of synaptic receptor activation, receptor saturation, and spill-over following quantal release.

MATERIALS AND METHODS

Use of the MCell simulation environment

Monte Carlo simulations were performed using MCell (Stiles and Bartol, 2001; Stiles et al., 2001; <http://www.mcell.cnl.salk.edu>). MCell uses Monte Carlo algorithms designed to simulate three-dimensional (3-D) Brownian random walk diffusion and uni and bimolecular reaction kinetics in complex spatial environments reflecting realistic cellular ultrastructure. Thus the impact of subcellular organization on the spatial and temporal evolution of biochemical diffusion/reaction systems can be studied using MCell. To model such a system it is necessary to specify 1) the geometry of the subcellular structures of the system, 2) the diffusion constants and initial locations of diffusing molecules, 3) the locations of transmembranous or scaffold-tethered effector molecules, 4) the reaction mechanisms and kinetic rate constants governing the interaction of diffusing molecules with effector molecules, and 5) an appropriate time step and number of iterations with which to simulate the spatial and temporal evolution of the system (Stiles and Bartol, 2001).

Ultrastructure of the synaptic cleft and neuropil

Glutamatergic synapses are thought to make up ~80% of all synapses in the central nervous system and occur mainly at dendritic spines (Harris and Kater, 1994). The pre and postsynaptic elements that comprise synapses of

the CNS are embedded within a complex cellular milieu known as neuropil. The present study is based on a simplified 3-D representation of a single synaptic spine, segment of dendrite, and surrounding neuropil which attempts to capture major anatomical and morphometric attributes of this system.

We modeled a $4 \mu\text{m} \times 4 \mu\text{m} \times 4 \mu\text{m}$ volume of simplified neuropil (with reflective boundary conditions) composed of cuboidal elements, $0.5 \mu\text{m}$ on a side, packed together in an $8 \times 8 \times 8$ element array with a 20-nm-thick gap of extracellular space surrounding each element (Fig. 1 A). The elements were thus packed on $0.52 \mu\text{m}$ centers, had a total intracellular volume of $64 \mu\text{m}^3$, an extracellular space percentage of ~10%, and a geometric tortuosity of 1.4 (see Chen and Nicholson, 2000; Fig. 1 D). Note that diffusion with this configuration is anisotropic, being fastest in the directions of the faces of the cubes. This is almost certainly not the case for more complex diffusion spaces, including actual neuropil, where the reflecting membrane surfaces are smaller and less regular.

Within this simplified neuropil matrix, we embedded a $4 \mu\text{m}$ segment of dendritic shaft with a square cross-section of $1 \mu\text{m} \times 1 \mu\text{m}$. The dendritic shaft had one synaptic spine consisting of a spine neck $0.5 \mu\text{m}$ long and $0.2 \mu\text{m} \times 0.2 \mu\text{m}$ in cross-section, and a cuboidal spine head $0.5 \mu\text{m}$ on a side. The presynaptic bouton consisted of a cuboid $0.5 \mu\text{m}$ on a side adjacent to the spine head, creating a 20 nm synaptic cleft (Fig. 1 B).

Although this structure is highly regular and simplified compared to natural neuropil, it offers several advantages over a faithful 3-D reconstruction of neuropil: it is simple to generate and characterize and is easy to visualize; its generation is parameterized and automated so that structural parameters may be modified and the physiological consequences explored; it is modular, allowing additional components of the diffusion/reaction system to be added with ease; and it allows a baseline of behavior for this diffusion/reaction system to be quantified under simplified condi-

TABLE 1 Rate constants describing the glutamate transporter kinetic model

Parameter	Symbol	Value	Primary Reference
Glutamate transporters			
Association rate constant	K_{TOT1}	$1.80 \times 10^7 \text{ M}^{-1} \text{ s}^{-1}$	Geiger et al., 1999
Dissociation rate constant	K_{T1T0}	180 s^{-1}	
Transition state rate constant	K_{T1T2}	180 s^{-1}	
Transport rate constant	K_{T2T0}	25.7 s^{-1}	

tions. Results obtained from simulations run in the neuropil were compared with similar simulations obtained from a simplified geometry consisting of two square sheets, 17 μm on a side, separated by 20 nm (hereafter “sheet”; Fig. 1 C).

Placement of receptors

Post-embedding immunogold methods (Matsubara et al., 1996) have shown AMPARs to have either a uniform distribution within the synaptic specialization (Nusser et al., 1994) or to be present in an annular structure around the center of the synapse (Matsubara et al., 1996; Kharazia and Weinberg, 1997). Takumi et al. (1999) reported that synapses with a diameter of <180 nm lack AMPARs, and that the number of AMPARs increases with synapse area, as shown both in hippocampal pyramidal cells (Nusser et al., 1998; Takumi et al., 1999; Racca et al., 2000) and the neocortex (Kharazia and Weinberg, 1999). By contrast, NMDARs were found on almost all asymmetric synapses in either CA1 (Takumi et al., 1999; Racca et al., 2000) or the neocortex (Kharazia and Weinberg, 1999), and their number only increases with synapse diameter (Takumi et al., 1999). Although NMDARs, across a population of synapses, occur more frequently in the center of the postsynaptic density (PSD) in hippocampus (Racca et al., 2000) and neocortex (Kharazia and Weinberg, 1997; Valtschanoff et al., 1999), this central localization may be the result of the central position of NMDARs in the large population of small synapses. In large hippocampal synapses, NMDARs may occur at any position along the PSD (Racca et al., 2000). We placed AMPARs and NMDARs within a 0.35- μm -diameter disk on the top surface of the spine head (Fig. 1 B) or in the center of the sheet (Fig. 1 C). The total density of receptors was varied in our study, but the “prototypical” case refers to a synapse containing 80 AMPARs and 20 NMDARs in Mg^{2+} -free solution. The distribution of both AMPARs and NMDARs across the PSD was uniform.

Glutamate transporters

Glutamate uptake, essential for returning extracellular glutamate levels to resting levels after the release of transmitter, is performed by a family of at least five different transporter proteins (Danbolt et al., 1998). Different types of transporters have been localized to hippocampal astroglia, Bergmann glia in the cerebellum, and on the postsynaptic membranes of CA1 pyramidal cells in the hippocampus and climbing fiber synapses in the cerebellum (Rothstein et al., 1994; Chaudhry et al., 1995; Lehre and Danbolt, 1998; Auger and Attwell, 2000). Lehre and Danbolt (1998) measured transporters at a density of 10,000 μm^{-2} on astroglia, which compose $\sim 10\%$ of the total membrane in CA1 neuropil. Thus, we have placed glutamate transporters on all membranes of the neuropil elements, at a density of 1000 molecules/ μm^{-2} .

Glutamate uptake from the extracellular space requires co-transport of 3 Na^+ and 1 H^+ ion, and the counter-transport of 1 K^+ ion (Zerangue and Kavanaugh, 1996; Levy et al., 1998), and complex reaction schemes have been proposed to describe its kinetics (Wadiche et al., 1995; Otis and Jahr, 1998; Auger and Attwell, 2000). After Diamond and Jahr (1997) and

Geiger et al. (1999) we used a simple three-state glutamate transporter reaction mechanism with four rate constants (see Table 1), with an apparent affinity of 20 μM (Arriza et al., 1994) and a slow turnover rate (Wadiche et al., 1995).

Release of glutamate

Evidence from high-resolution two-electrode voltage-clamp studies and computer modeling of miniature endplate current (MEPC) time-course at the neuromuscular junction suggests that MEPC rise-time is so short that the time course of vesicle emptying must be extremely rapid (Stiles et al., 1996). We therefore modeled glutamate release as an instantaneous point source centered over the postsynaptic receptor patch. Unless otherwise stated, we assumed a glutamate diffusion coefficient (D_{Glu}) of 0.2 μm^{-2} , slowed to approximately one-third that of aqueous glutamine (Longworth, 1953) due to molecular overcrowding (Bartol, 1992; Elowitz et al., 1999; Ellis, 2001), but see Barbour (2001).

Simulation time step

The numerical accuracy of MCell simulations depends primarily on the duration of the simulation time step (Stiles and Bartol, 2001). The time step affects the average diffusion step-length and the probability of reaction events. Validation of MCell’s Monte Carlo algorithms has shown that the average radial diffusion step-length should be no larger than $\sim 1/2$ the radius of any diffusion barrier bottlenecks, and that simulation accuracy of 99% or better can be achieved with probabilities of <0.2 for reaction events (Stiles and Bartol, 2001). In the present study a simulation time step of 1 μs was used to satisfy these conditions.

The parameter values specified above represent the mean values used. At initialization of each simulation, the exact number and positions of receptors and uptake sites were randomly assigned on specified surfaces (Stiles and Bartol, 2001). Simulations were run on a cluster of 933 MHz PC workstations running FreeBSD 4.0. It took ~ 20 min of computer time to simulate 1 s of real time; 3-D images were rendered with IBM Data Explorer (<http://www.openfx.com>) using custom-written software (DReAMM, Joel Stiles, <http://www.mcell.psc.edu/DReAMM>). Parameters are taken from experiments performed at room temperature, and output of the model is therefore a simulation of these conditions. Data are presented as mean \pm standard deviation unless otherwise specified.

RESULTS

Time course of glutamate concentration

Experimental estimates of the time course of synaptic glutamate concentration ($[\text{Glu}]_{\text{left}}$) based on competition with low-affinity competitive antagonists suggest a peak concentration of 1–3 mM and a biphasic decay, with a fast decay constant of $\sim 100 \mu\text{s}$ and a slower decay constant of ~ 1 ms (Clements et al., 1992; Tong and Jahr, 1994; Clements,

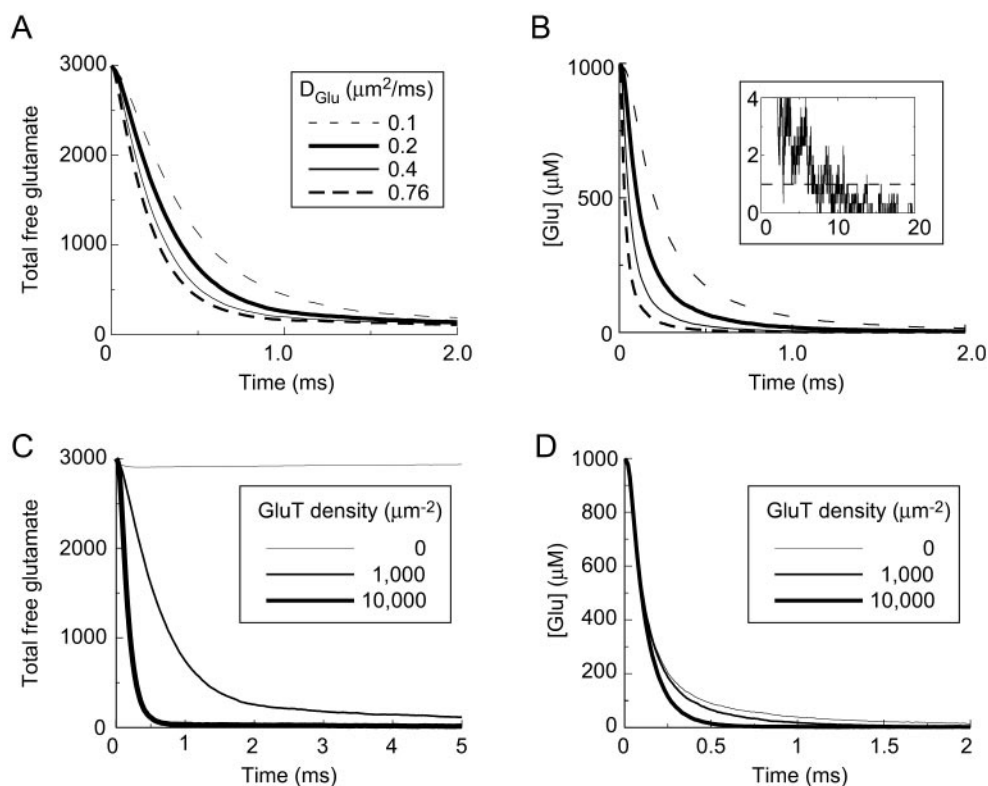


FIGURE 2 Time course of glutamate. (A) Average number (20 trials) of free glutamate molecules remaining in the entire extracellular space of the neuropil. Uptake is sensitive to the diffusion rate of glutamate. (B) Concentration of free glutamate in the synaptic cleft after release also depends on glutamate diffusion rate. Legend as in A. *Inset*: single trial showing free synaptic glutamate as concentration decreases toward K_D of NMDAR (*dashed line*). The decay rate of glutamate in the neuropil (C), but not the cleft (D), is very sensitive to the density of transporters.

1996; Diamond and Jahr, 1997). We released a quantum of transmitter (3000 molecules) as a point source at the center of the synaptic cleft and the resulting decay of glutamate in the neuropil was biphasic, with time constants of 609 μ s (93%) and 6.1 ms (fit range: 20 ms; Fig. 2 A). Because we did not place glutamate transporters in the synaptic cleft, $[Glu]_{\text{cleft}}$ remained roughly constant for approximately the first 10 μ s after release. Transmitter levels in the cleft then fell precipitously from millimolar concentrations to submicromolar concentrations, with a biphasic decay with time constants of 122 μ s (91%) and 623 μ s (Fig. 2 B). Diamond and Jahr (1997) report a double-exponential decay with similar decay constants to those reported here. However, their peak concentration (~ 4 mM) was higher, and their slow component (14%) larger, than our simulations predict, possibly reflecting errors introduced by the simplifying assumption of instantaneous glutamate release used in both cases. Binding of transmitter to uptake sites roughly matched the time course of free glutamate in the cleft, although we did not attempt to derive transporter currents (Bergles et al., 1997; Auger and Attwell, 2000) from our simplistic uptake scheme.

Unlike the neuromuscular junction, where the action of acetylcholine is terminated by rapid enzymatic degradation

(Eccles et al., 1942), the time course of glutamate concentration must be a function of rapid diffusion out of the cleft (Eccles and Jaeger, 1958; Wahl et al., 1996) and/or uptake via glutamate transporters (Danbolt et al., 1998; Diamond, 2001). Although transporter kinetics are relatively slow (Wadiche et al., 1995), rapid binding and buffering of glutamate by transporters may help shape the time course of the synaptic glutamate transient (Diamond and Jahr, 1997). Decreasing D_{Glu} increased the fast and slow components of the decay in both the entire neuropil (Fig. 2 A) and the synaptic cleft (Fig. 2 B) due to the slowing of the diffusion of glutamate from the center of the synapse. Note the similarity between the time course of free glutamate in the cleft, where there were no uptake sites, and in the entire neuropil, where there was a high density of uptake sites, suggesting that most glutamate was immediately absorbed on leaving the cleft.

Although astrocytes have a high density of glutamate transporters, $<50\%$ of the synapses in the CA1 region of the hippocampus are covered by astrocytic membrane (Ventura and Harris, 1999). The dynamics of neuropilar glutamate were therefore examined with three different transporter densities: 1000 μm^{-2} simulated the *average* case; 10,000 μm^{-2} simulated the case in which a synapse was com-

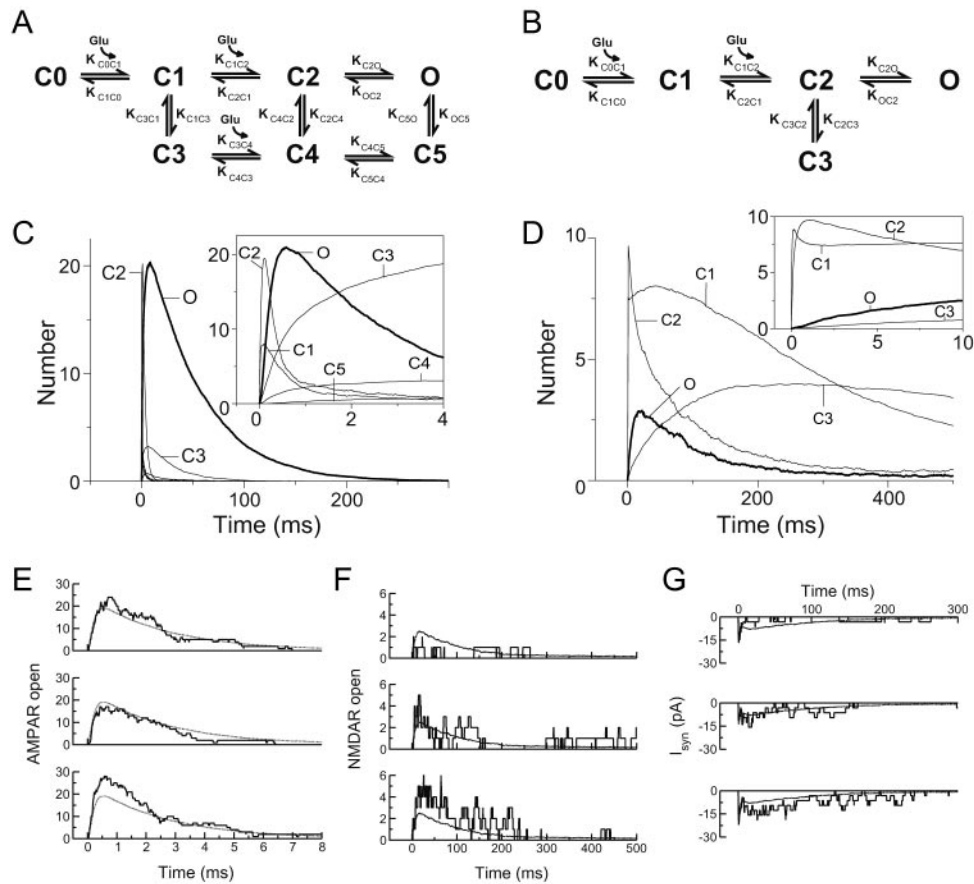


FIGURE 3 Receptor activation after quantal release. Kinetic scheme used for AMPARs (A) and NMDARs (B). Time course of AMPAR (C) and NMDAR (D) activation pathways (ensemble averages, $n = 150$). *Insets*: expanded view of early events in activation pathway. Note the rapid onset to the C1 and C2 states of both receptor types; the difference in rise-times between AMPARs and NMDARs was determined by their transition rates from C2 to O. Single trial variability in AMPAR (E) activation, NMDAR (F) activation, and total synaptic current (G) are plotted with the ensemble averages (*thin lines*). Traces across each row show results from the same simulation.

pletely ensheathed by astrocyte membrane; and $0 \mu\text{m}^{-2}$ simulated the case in which there was no astrocytic membrane between or near the release site(s) and the synapse, or in which transporters were pharmacologically blocked. Changing the density of glutamate transporters dramatically altered the clearance of glutamate from the neuropil (Fig. 2 C), but had a much smaller effect in the cleft (Fig. 2 D), altering the time course by changing the probability that a glutamate molecule that left the cleft would diffuse back in before being bound by transporter.

Evolution of receptor states

After release, transmitter diffused across the synaptic cleft and activated AMPARs and NMDARs. We implemented a reaction scheme and set of kinetic rate constants for AMPARs from Jonas et al. (1993; see Fig. 3 A and Table 2) and NMDARs from Lester and Jahr (1992; see Fig. 3 B and Table 3). Before release, all receptors were in the C0 state. Upon binding glutamate, the receptors changed states ac-

cordingly (Fig. 3, C and D). The ensemble average (average of 250 traces) of open AMPARs peaked at 21 ± 5.2 (26% of receptor population), 580 μs after release; 20%–80% rise-time 206 μs . The decay of the number of open AMPARs could be fit with a single-exponential time constant of 2.6 ms. Like the AMPARs, the single- (C1) and double-liganded (C2) closed states of the NMDARs evolved extremely rapidly; 20%–80% rise-times were 32 μs and 215 μs , respectively (Fig. 3 C). Unlike AMPARs, however, the extremely slow opening rate dramatically slowed the opening of NMDARs. The ensemble average of open NMDARs peaked at 3.3 ± 1.8 (15% of the receptor population), 21 ms after release; 20%–80% rise-time of 7.3 ms; double-exponential decay time constants of 77 ms (88%) and 862 ms. NMDARs desensitized slowly, with a peak of 4.0 desensitized receptors.

Each simulation, starting with a different random number generator seed, produced a different number and distribution of receptors, and random walk trajectory of glutamate (Stiles et al., 2001; Stiles and Bartol, 2001), yielding vari-

TABLE 2 Rate constants describing the AMPA receptor kinetic model

Parameter	Symbol	Value	Primary Reference
Glutamate			
Diffusion coefficient	D_{Glu}	$0.2 \mu\text{m}^2 \text{ms}^{-1}$	
AMPA receptors			
First association rate constant	K_{C0C1}	$4.59 \times 10^6 \text{M}^{-1} \text{s}^{-1}$	Jonas et al., 1993
First dissociation rate constant	K_{C1C0}	$4.26 \times 10^3 \text{s}^{-1}$	
Second association rate constant	K_{C1C2}	$2.84 \times 10^3 \text{M}^{-1} \text{s}^{-1}$	
Second dissociation rate constant	K_{C2C1}	$3.26 \times 10^3 \text{s}^{-1}$	
Channel opening rate constant	K_{C2O}	$4.24 \times 10^3 \text{s}^{-1}$	
Channel closing rate constant	K_{OC2}	900s^{-1}	
C1 to C3 desensitization rate constant	K_{C1C3}	$2.89 \times 10^3 \text{s}^{-1}$	
C3 to C1 resensitization rate constant	K_{C3C1}	39.2s^{-1}	
C3 to C4 association rate constant	K_{C3C4}	$1.27 \times 10^6 \text{M}^{-1} \text{s}^{-1}$	
C4 to C3 dissociation rate constant	K_{C4C3}	45.7s^{-1}	
C2 to C4 desensitization rate constant	K_{C2C4}	172s^{-1}	
C4 to C2 resensitization rate constant	K_{C4C2}	0.727s^{-1}	
C4 to C5 isomerization rate constant	K_{C4C5}	16.8s^{-1}	
C5 to C4 isomerization rate constant	K_{C5C4}	190.4s^{-1}	
Open to C5 desensitization rate constant	K_{OC5}	17.7s^{-1}	
C5 to Open resensitization rate constant	K_{C5O}	4.0s^{-1}	

able responses. The peak number of open receptors was AMPARs, 23 ± 4.3 (C.V. 19%; Fig. 3 *E*); NMDARs, 4.9 ± 1.6 (C.V. 33%; Fig. 3 *F*). Assuming single channel conductance values of 10 pS for AMPARs and 45 pS for NMDARs (Spruston et al., 1995), the average peak total conductance was 198 pS, corresponding to a 14 pA current assuming a holding potential of -70 mV (Fig. 3 *G*). The peak of the NMDAR component, at 14 ms, was 56% of the AMPAR peak. Because of their slow kinetics and large single channel conductance, NMDARs contributed 96% of the total accumulation of charge following quantal release. Note that the NMDA currents were simulated in the absence of Mg^{2+} , giving large values for the NMDA component.

Parameter sensitivity

To address the dependence of receptor activation on n and q we independently varied these two variables. Increasing n in a constant AMPAR/NMDAR ratio of 4:1 (AMPAR range 14–905; NMDAR range 4–226) linearly increased the number of open AMPARs (Fig. 4 *A*) and NMDARs (Fig. 4 *B*), implying that there was no cooperativity among the recep-

tors. Because the binding of two transmitter molecules was required to open a single receptor, receptor activation decreased at very high receptor densities when the total number of receptors approached the total number of transmitter molecules released and receptors had to compete for limiting amounts of transmitter (data not shown). This might reflect the situation at dendritic receptors where much higher numbers of receptors have been reported (Jonas et al., 1993; Spruston et al., 1995; Andrasfalvy and Magee, 2001), but the number of receptors necessary to produce competition is too large to be physiologically relevant at spinous synapses.

Fig. 4, *A* and *B* suggest the activation of individual receptors was independent of other receptors at the synapse when the synaptic ratio of NMDAR/AMPAR was fixed. However, the number of NMDARs appears to be relatively stable, while the number of AMPARs increases with the size of the synapse (Takumi et al., 1999). Thus, the high affinity of NMDARs for transmitter might either amplify the activation of AMPARs via buffered diffusion or decrease their activation through competition, when the number of NMDARs is much greater than the number of AM-

TABLE 3 Rate constants describing the NMDA receptor kinetic model

Parameter	Symbol	Value	Primary Reference
NMDA receptors			
First association rate constant	K_{C0C1}	$2 \times 5.0 \times 10^6 \text{M}^{-1} \text{s}^{-1}$	Lester and Jahr, 1992
First dissociation rate constant	K_{C1C0}	4.7s^{-1}	
Second association rate constant	K_{C1C2}	$5.0 \times 10^6 \text{M}^{-1} \text{s}^{-1}$	
Second dissociation rate constant	K_{C2C1}	$2 \times 4.7 \text{s}^{-1}$	
Channel opening rate constant	K_{C2O}	46.5s^{-1}	
Channel closing rate constant	K_{OC2}	91.6s^{-1}	
C2 to C3 desensitization rate constant	K_{C2C3}	8.4s^{-1}	
C3 to C2 resensitization rate constant	K_{C3C2}	1.8s^{-1}	

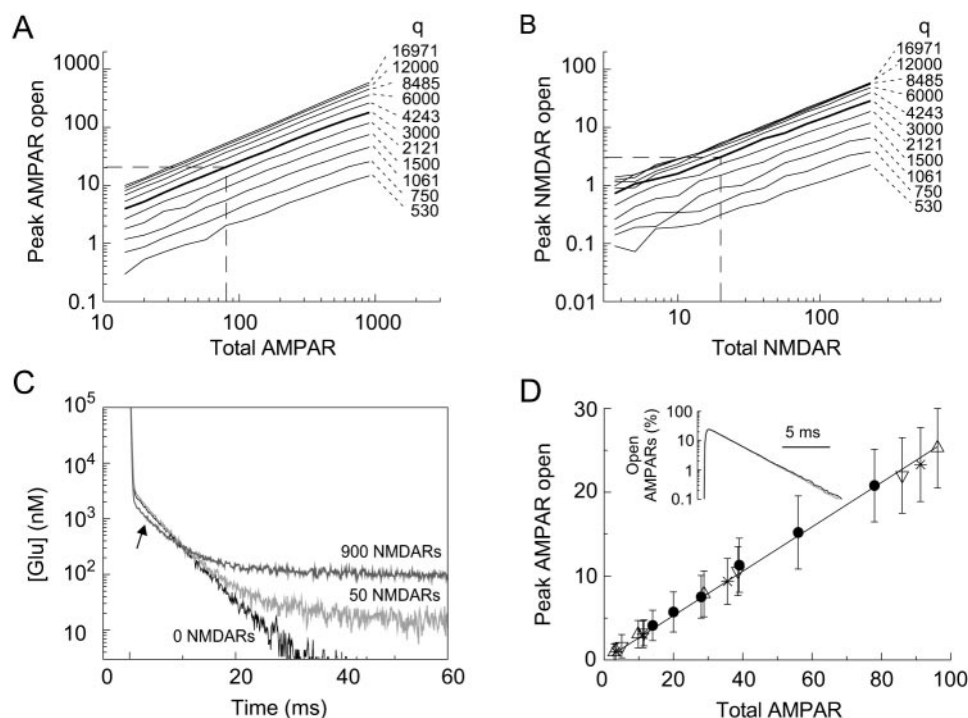


FIGURE 4 Activation of AMPARs and NMDARs scale linearly with receptor number. Number of AMPARs (A) or NMDARs (B) open at peak as a function of total number of receptors. Each line represents this relationship for a different quantal size. The bold line indicates the response with 3000 glutamate molecules per quantum; the dotted line marks the central case of 80 AMPARs and 20 NMDARs. (C) Decay of average synaptic glutamate concentration ($n = 300$) was slowed by high densities of NMDARs. At very high, nonphysiological NMDAR densities (900 per synapse), free [Glu] was transiently decreased as transmitter bound receptors (arrow), but therefore could not clear the synapse, resulting in a more substantial increase in a sustained free [Glu] (~ 100 nM), as glutamate later dissociated from NMDARs. (D) AMPAR activation did not depend on the number of co-localized NMDARs at the same synapse: \bullet 20 NMDARs; \triangle 30 NMDARs; ∇ 40 NMDARs; $*$ 50 NMDARs. The straight line shows a linear fit to all data with a slope of 0.264, $r^2 > 0.99$. Inset: semilogarithmic plot showing identical decay of averaged open AMPARs ($n = 300$) co-localized with 0 (black trace) or 50 NMDARs (gray trace).

PARs, for example at developing synapses (Liao et al., 1995; Isaac et al., 1995; Wu et al., 1996).

To first demonstrate the buffered diffusion of transmitter in the cleft we averaged a large number of trials ($n = 300$) measuring synaptic glutamate concentration under three conditions: with no receptors, in which glutamate was free to diffuse out of the cleft; with 50 NMDARs and 80 AMPARs, representing a synapse with high NMDAR content in which we might see buffered diffusion; and with 900 NMDARs and 50 AMPARs (limited by the number of receptors that could be packed at the synapse, Fig. 4 C). The initial fast decay of transmitter was similar in all three cases. When populated by an extremely high number of NMDARs, $[Glu]_{\text{cleft}}$ undershot control levels because a large fraction of transmitter was bound and therefore no longer free. However, whenever a glutamate molecule dissociated from a receptor, $[Glu]_{\text{cleft}}$ increased incrementally. Thus, populating the synapse with NMDARs resulted in a small but sustained increase in average $[Glu]_{\text{cleft}}$. Note, however, that the concentration of a single free glutamate in the cleft (volume, 5 aL) was $0.33 \mu\text{M}$. Thus, an average $[Glu]_{\text{cleft}}$ of 15 nM (well below background glutamate lev-

els) really means that the probability of having a single free transmitter molecule in the cleft was 0.05—suggesting that although high densities of NMDARs could buffer the diffusion of synaptic glutamate, the effect would be too small to be functionally significant.

To explicitly test this with physiological receptor densities, we compared the peak number of open AMPARs as a function of total AMPARs, but co-localized with a fixed number of NMDARs. The relationship was always linear (i.e., a constant fraction of AMPARs, 26%, was opened by a quantum of transmitter). Moreover, this relationship was identical at synapses with different NMDAR content (range, 20–50 NMDARs, Fig. 4 D). The peak number of open receptors was mainly driven by the initial binding event (also see below), but buffered diffusion slowed the rate of decay rather than increased the peak of $[Glu]_{\text{cleft}}$, so synapses with high NMDAR content may prolong AMPAR currents. We therefore also looked at the kinetics of the decay of the ensemble average of open AMPARs, which were identical whether expressed alone or co-localized with 50 NMDARs (Fig. 4 D, inset). Therefore, the activation of synaptic receptors was independent of other receptors co-

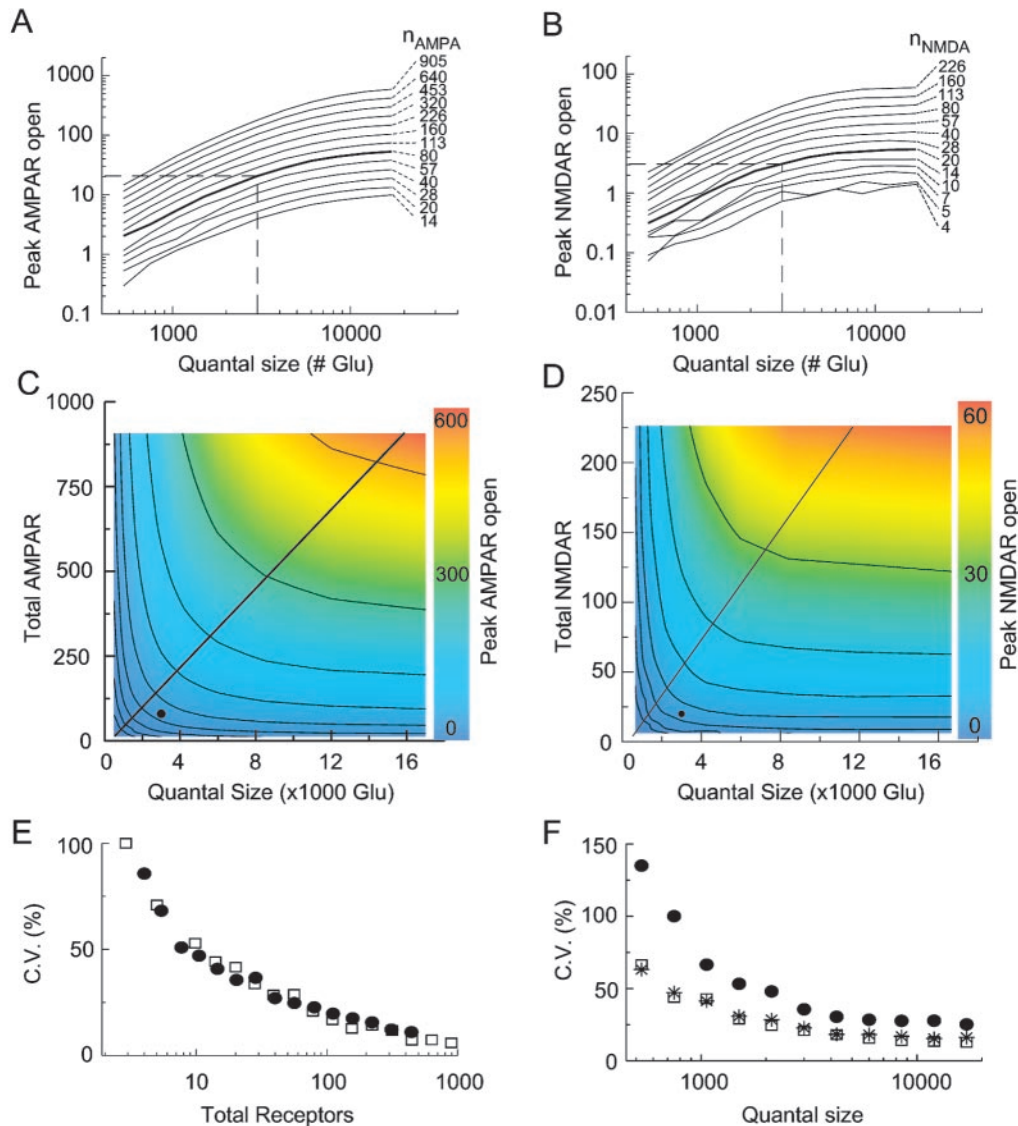


FIGURE 5 Increasing quantal size resulted in a sublinear increase in peak number of open AMPARs (A) and NMDARs (B) due to partial saturation of receptors at high quantal values. Each line represents the response for a different total number of receptors. Bold lines indicate the response with 80 AMPARs and 20 NMDARs; the dotted line marks the central case. Sensitivity of peak number of open AMPARs (C) or NMDARs (D) to quantal size and total receptor number is shown. The marker indicates the point of 80 AMPARs and quantal size of 3000 glutamate. The peak in open AMPARs and NMDARs was most sensitive to change in total receptor number in the region of parameter space below the diagonal line and most sensitive to change in quantal size in the region above the line. (E) Quantal variability decreased with increasing numbers of receptors ($q = 3000$). There was little difference between the variability in AMPAR activation (\square) and (\bullet) NMDAR activation with similar population sizes. (F) Variability as a function of quantal size: \square $n_{\text{AMPA}} = 80$; \bullet $n_{\text{NMDA}} = 20$; * $n_{\text{NMDA}} = 80$.

localized at the same synapse, and an increase in AMPAR number translates linearly to an increase in the AMPA response.

Increasing q from ~ 500 to 17,000 glutamate molecules per vesicle increased the activation of both AMPARs (Fig. 5 A) and NMDARs (Fig. 5 B). However, the potency of incremental increases in q decreased due to receptor saturation. Therefore, the sensitivity to changes in receptor number and quantal size depends strongly on the initial configuration of the synaptic system in n and q

parameter space. These data are summarized for AMPARs (Fig. 5 C) and NMDARs (Fig. 5 D). Receptor activation was most sensitive to changes in n at points below the diagonal line (i.e., when quantal size was large relative to total receptor number) and most sensitive to changes in q at points above the diagonal line (i.e., when quantal size was small relative to total receptor number). The case we have used for the central condition (i.e., $q = 3,000$; $n_{\text{AMPA}} = 80$, $n_{\text{NMDA}} = 20$) lies below the diagonal line, thus favoring change in total receptor number as the

most sensitive means to modulate individual synaptic efficacy.

The trial-to-trial variability in the responses of a population of AMPARs (Fig. 3 *E*) or NMDARs (Fig. 3 *F*) decreased with increasing size of the receptor pool (Fig. 5 *E*). Despite their very different kinetics, the variability in AMPAR and NMDAR activation to a quantum of transmitter were almost identical for a given receptor pool size. Variability also decreased with increasing quantal size, again with almost identical C.V.s of the AMPAR and NMDAR responses with equal numbers of receptors (Fig. 5 *F*).

Receptor saturation

A question of fundamental importance in synaptic physiology is the degree to which postsynaptic receptors are saturated following quantal release. Because of the large number of glutamate molecules released (Clements et al., 1992; Tong and Jahr, 1994; Diamond and Jahr, 1997) into the small volume of the synaptic cleft, it has traditionally been assumed that receptors, in particular the high-affinity NMDARs, were saturated following the release of a single vesicle (reviewed in Frerking and Wilson, 1996). However, recent experiments suggest that these receptors are not saturated (Liu et al., 1999; Mainen et al., 1999; McAllister and Stevens, 2000). Occupancy is defined here as the percentage of the total pool of either AMPARs or NMDARs that have both their glutamate binding sites occupied. Release of 3000 molecules of transmitter across from 80 AMPARs and 20 NMDARs resulted in low, and similar, levels of peak occupancy for both AMPARs (38%) and NMDARs (54%, Fig. 6). Because the total number of receptors was much smaller than the quantal size, both AMPAR and NMDAR occupancy were only weakly dependent on n (Fig. 6, *A* and *B*) but were strongly dependent on q (Fig. 6, *C* and *D*).

Temporal dependence of signaling

In addition to determining the response to the instantaneous application of different sized quanta, we simulated the sequential release of five quanta of 3000 molecules at 100 Hz. Their fast kinetics allowed AMPARs to peak and decay, almost to resting levels, before release of the next quantum. However, because each quantum resulted in some receptor desensitization, each subsequent response was depressed (Fig. 7 *A*). The 100 Hz train resulted in an increase in the NMDAR response with each additional quantum until the response plateaued after four quanta (Fig. 7 *B*). A recent study measured a paired-pulse ratio of 0.8 for NMDA currents at single synapses with a 10 ms interstimulus interval. From this the authors concluded that NMDARs can be no more than 56% occupied following quantal release (Mainen et al., 1999). We obtained a similar paired-pulse

ratio of 0.73 with the same pairing interval (data for only two release events, not shown).

The rapid dissociation of AMPARs prevented the accumulation of saturated AMPARs during multiple release events (Fig. 7 *C*). By contrast, the slow dissociation rate of the NMDARs resulted in a steplike increase in saturation with the release of each additional quantum (Fig. 7 *D*). Furthermore, NMDAR saturation levels following release of each quantum were almost identical to saturation levels after instantaneous release of larger quantal sizes (Fig. 6 *D*). Our simulations therefore suggest saturation of NMDARs would not be significant until release of $\sim 10,000$ glutamate molecules. Therefore, due to the differences in their dynamics of saturation, AMPARs are able to act largely as differentiators, responding to rapid changes in synaptic glutamate levels, whereas NMDARs act as leaky integrators, tracking the total amount of transmitter released over a sustained interval. The desensitization of AMPARs and the slow off-rate of NMDARs therefore preclude temporally independent signaling.

Glutamate diffusion

The concentration of transmitter in the synaptic cleft was sensitive to D_{Glu} (Fig. 2 *B*). The effect of changing D_{Glu} on peak opening and saturation levels were determined under central conditions. Increasing D_{Glu} decreased both the peak number of open receptors (Fig. 8 *A*) and receptor saturation levels (Fig. 8 *B*). Receptor activation and saturation levels were low when the values for D_{Glu} approached the rate for aqueous glutamine, but increased dramatically as D_{Glu} was decreased. Note that the relative saturation of NMDARs to AMPARs increased as D_{Glu} decreased.

Role of glutamate uptake and tissue morphology

Increasing or decreasing uptake had a smaller effect on the time course of synaptic glutamate concentration in the neuropil than in the sheet (Fig. 9 *A*), as glutamate was less likely to diffuse back into the cleft due to the greater tortuosity of the diffusion space. Blocking glial glutamate uptake therefore had little effect on peak activation levels and no effect on the kinetics of the AMPAR response in the neuropil (Fig. 9 *B*), consistent with experimental findings in hippocampal slices (Hestrin et al., 1990; Isaacson and Nicoll, 1993; Sarantis et al., 1993). However, in the sheet, blocking uptake resulted in a greater increase in peak AMPAR activation, and blocking uptake caused a slowing of the AMPAR decay ($\tau = 3.1$ ms; Fig. 9 *C*). Blocking uptake resulted in slightly increased peak levels of NMDAR activation in the neuropil (Fig. 9 *D*) and greatly increased levels in the sheet (Fig. 9 *E*). In both cases, blocking uptake affected the kinetics of the NMDAR response (Fig. 9, *D* and *E*). These results suggest the tortuosity of the neuropil plays a crucial role in terminating the synaptic response in the

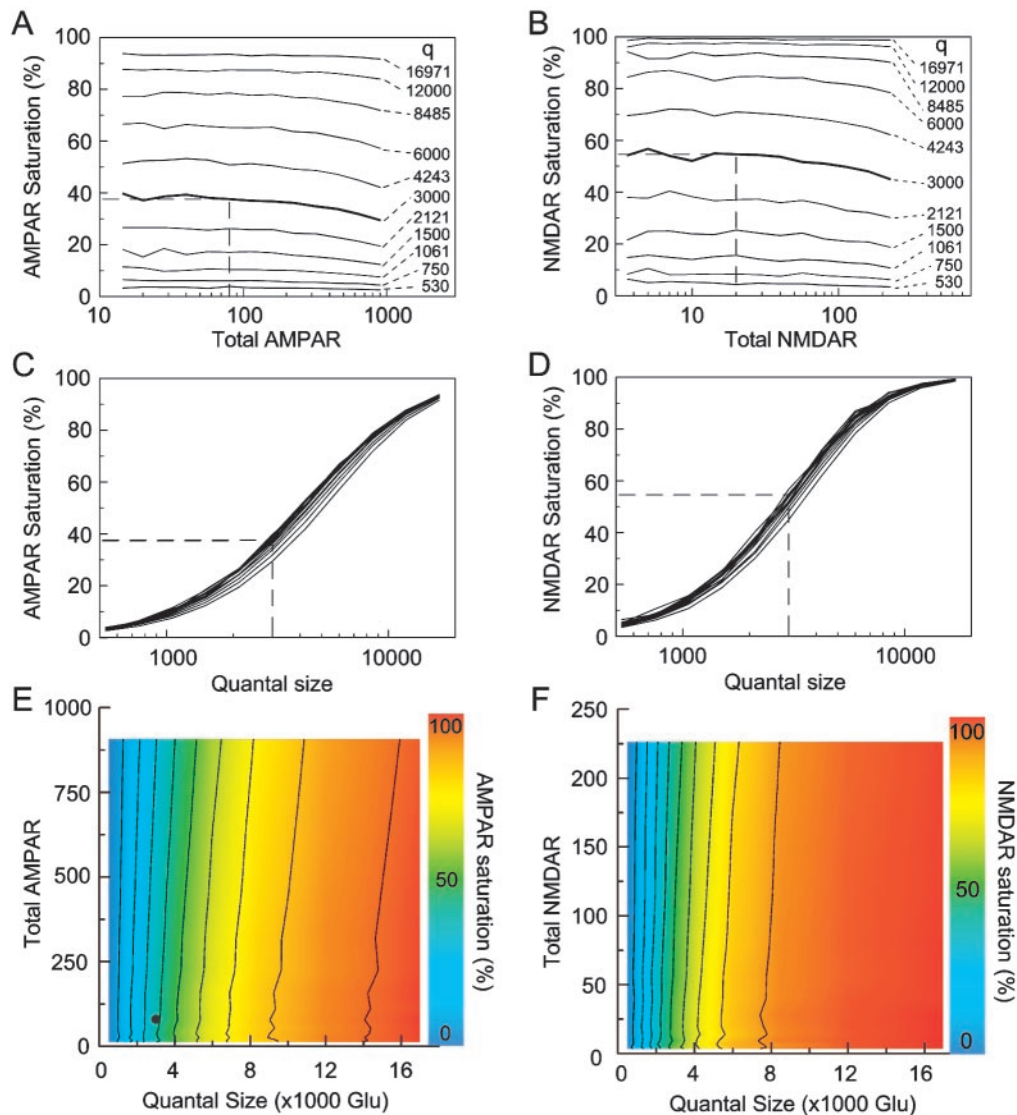


FIGURE 6 AMPAR and NMDAR saturation. Saturation of AMPARs (A) and NMDARs (B) was not sensitive to the size of the receptor pool. Each line represents the saturation level at a different quantal size. Bold lines indicate the response with 3000 glutamate molecules per quantum; the dotted line marks the central case. Receptor saturation was strongly dependent on quantal size. Saturation levels for AMPARs (C), through a range from 14 to 905 receptors, or NMDARs (D), through a range from 4 to 226 receptors, with increasing quantal size, are shown. Dotted lines mark the central case. AMPAR (E) and NMDAR (F) saturation levels were almost solely due to quantal size and largely insensitive to receptor number. The marker indicates quantal size of 3000 glutamate and 80 AMPARs or 20 NMDARs.

absence of uptake and predicts that receptor activation will increase when uptake is blocked in tissues with significantly lower tortuosity, such as the chick ciliary ganglion, or in which glutamate clearance from the cleft is physically restricted, such as at the parallel fiber-Purkinje cell synapse.

Glutamate spillover and activation of extrasynaptic receptors

Following release of glutamate in the synapse the uptake of extracellular glutamate under central conditions, or with slowed or blocked uptake, are described above and shown in

Fig. 2 C. To better conceptualize these data, we have rendered 3-D *snapshots* of the synapse at three times after release for each of these conditions, showing how the density of uptake sites restricted the temporal and spatial extent of extrasynaptic glutamate (Fig. 10, also see supplemental information; http://www.cnl.salk.edu~franks/ftp/spillover_movies/).

The functional consequence of this spillover was examined by releasing one quantum of glutamate above a neighboring cuboid element, $0.5 \mu\text{m}$ from the center of the cleft. There was no activation of postsynaptic receptors in the presence of either high (data not shown) or normal densities

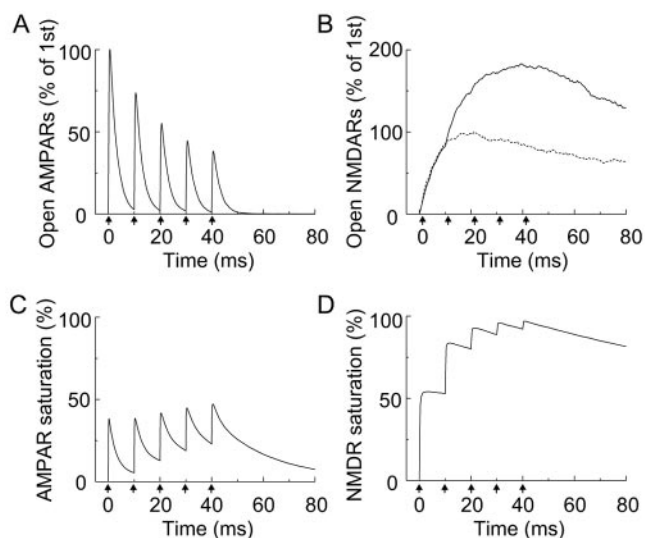


FIGURE 7 Temporal dependence of transmitter exposure. (A) Desensitization decreases potency of AMPARs to subsequent release events. Arrows mark the release of each quantum, whereas the number of open NMDARs (B) increases with additional transmitter. (C) Saturation levels of AMPARs do not increase during a high-frequency train. (D) The long dissociation rate of NMDARs results in increased saturation levels after multiple release events. The dashed line shows response to a single quantum.

of glutamate transporters (Fig. 11 A). In the absence of uptake there was a low level of NMDAR activation. Simultaneous release of four quanta, equidistant but on different sides of the synapse, still failed to activate synaptic recep-

tors with a high density of uptake sites, but otherwise resulted in mild activation of both AMPA and NMDA receptors (Fig 1 D). Extrasynaptic receptor action with transporter density doubled ($2000 \mu\text{m}^{-2}$) or halved ($500 \mu\text{m}^{-2}$) was not significantly different from the control condition ($1000 \mu\text{m}^{-2}$, data not shown). Without uptake, simultaneous release of four quanta, resulting in a resting [Glu] of $1.6 \mu\text{M}$, activated NMDARs, but also led to a high level of receptor desensitization (Fig. 11 B).

The degree to which the tortuosity of the neuropil prevented activation of extrasynaptic receptors was determined by comparing these results to simulations run in the sheet. A quantum of transmitter was released at a radial distance of $1.2 \mu\text{m}$ from the center of the synapse, equivalent to the minimum city-block metric length from the release site to the synapse in the cuboid neuropil. A high density of glutamate uptake sites continued to prevent any extrasynaptic glutamate activation of synaptic receptors (data not shown). Although the final resting levels of transmitter were similar in the neuropil and the sheet when uptake was blocked, decreasing transporter density in the sheet resulted in a large spike in cleft glutamate concentration (Fig. 11 C). This brief spike was sufficient to produce substantially higher levels of extrasynaptic receptor activation following the release of one (Fig. 11 C) or four quanta (Fig. 11, C and D). Note that in the model all transporters were initially unoccupied and therefore available to bind glutamate. Given their slow turnover rates (Wadiche et al., 1995), and the high density of synapses in CA1 neuropil (Harris and Kater, 1994), our results therefore overestimate the efficiency of uptake.

DISCUSSION

Glutamate time course, uptake, and spillover

The decay $[\text{Glu}]_{\text{cleft}}$ was a function of the speed at which glutamate could diffuse out of the cleft, and was largely insensitive to transporter density. At very high transporter densities, such as might be expected for a synapse ensheathed in astrocytic membrane, most of the glutamate was rapidly bound upon leaving the cleft, limiting the spatial extent and lifetime of the transmitter. Experimental studies have shown that blocking uptake with dihydrokainate (DHK) resulted in a slightly increased peak activation and no change in the kinetics of evoked NMDA currents (Hestrin et al., 1990). However, DHK is not an efficacious blocker of uptake (Ferkany and Coyle, 1986; Barbour et al., 1991). *L-trans*-PDC, a more potent blocker of glutamate uptake, either had no effect on the peak or kinetics of evoked NMDA currents (Isaacson and Nicoll, 1993), or resulted in a greatly decreased NMDA current (Sarantis et al., 1993), presumably due to receptor desensitization following an increase in extracellular glutamate. We did not see NMDAR desensitization in our simulations because we examined only the response to a single release of transmitter, with no previous glutamate exposure. However, the fraction of NMDARs in our model that were desensitized following release of four quanta

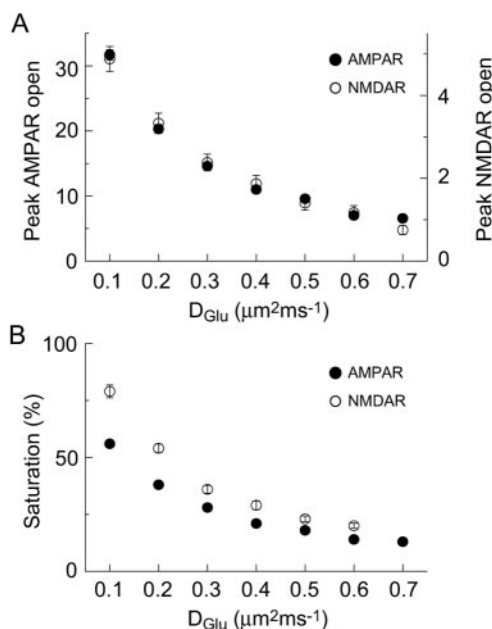


FIGURE 8 Rate of transmitter diffusion dramatically affects both efficacy (A) and saturation (B) of AMPA and NMDA receptors. Data are given as mean \pm standard error ($n > 50$).

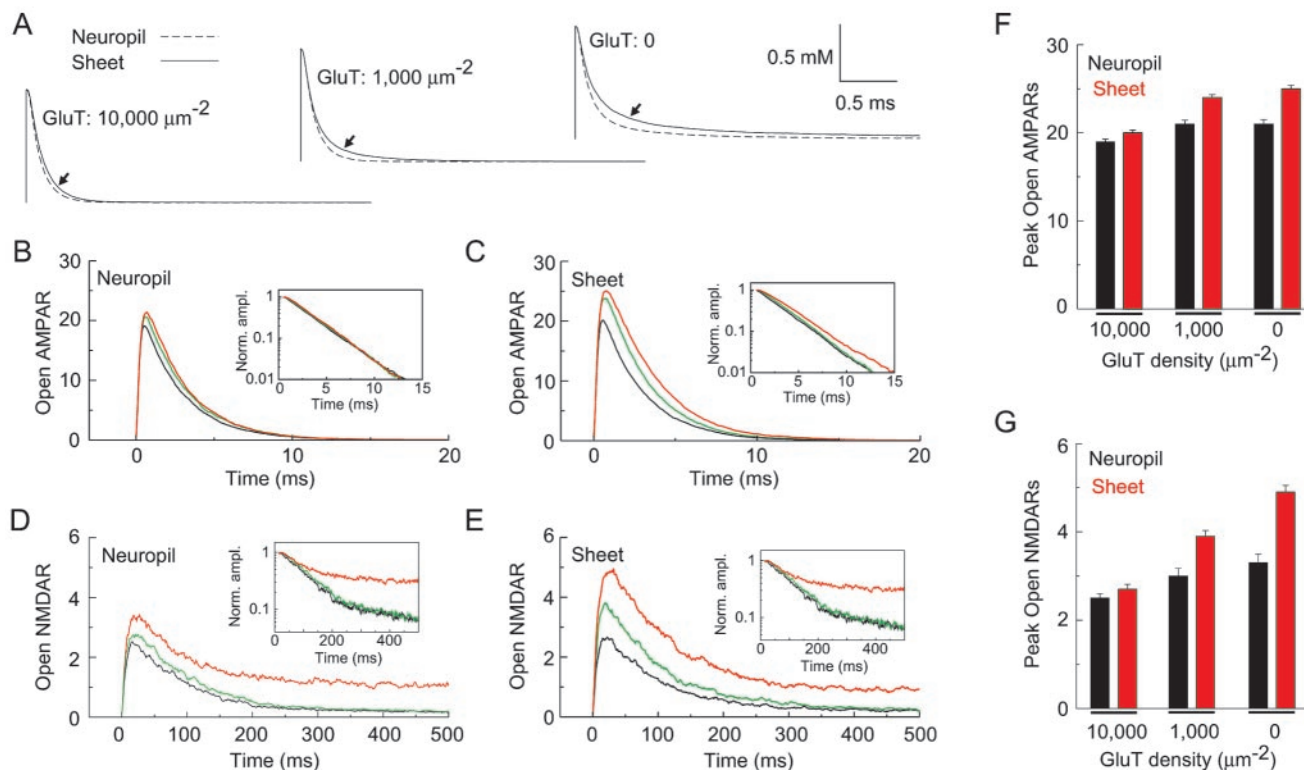


FIGURE 9 Geometry determines receptor sensitivity to glutamate uptake. (A) Glutamate transients in the cleft of the neuropil and sheet with different densities of uptake sites. Note the glutamate transient in the sheet is more sensitive to decreased uptake. (B) Peak AMPAR activation was largely insensitive to uptake density. (GluT density: $10,000 \mu\text{m}^{-2}$, black trace; $1,000 \mu\text{m}^{-2}$, green trace; $0 \mu\text{m}^{-2}$, red trace.) Inset: semilogarithmic plot showing the decay of the normalized amplitudes of open AMPARs. (C) As in B, but in the sheet. Note the greater sensitivity of both peak and decay of AMPARs to uptake in this configuration. (D) As in B, but showing the activation and time course of NMDARs in the neuropil. Note the small increase in peak activation and the change in kinetics with blocked, but not slowed, uptake. (E) As in D, but in the sheet. Note the greater sensitivity of peak NMDAR activation with slowed or blocked uptake. (F) Summary of peak AMPAR activation in the neuropil and sheet as a function of glutamate uptake rate. Data are given as mean \pm standard error. (G) Summary of peak NMDAR activation in the neuropil and sheet as a function of glutamate uptake rate. Data are given as mean \pm standard error ($n = 10$).

suggest a much smaller response to subsequent release, and results consistent with Sarantis et al. (1993).

Receptor activation

Glutamate bound to both AMPARs and NMDARs within microseconds of its release, whereas the number of open receptors peaked at $500 \mu\text{s}$ and 21 ms after release, respectively. This difference was due to the slow opening rate of NMDARs rather than to prolonged access of the high-affinity NMDARs to lower concentrations of transmitter in the cleft, confirming experimental predictions (Hestrin et al., 1990; Lester et al., 1990). Our simulations also predict a small but significant degree of AMPAR desensitization following quantal release, contrary to experimental reports from CA1 pyramidal cells (Stevens and Wang, 1995; Hjelmstad et al., 1997). This discrepancy may be due to either experimental errors or to errors in the assumptions in our model. For example, the AMPAR kinetic scheme used in this model was derived from excised patches of CA3

somata but is compared to physiological recording from CA1 spinous synapses. Furthermore, the receptor state models used in these simulations do not reflect the true complexity of receptor activation, particularly concerning heterogeneous populations of receptor subtypes, multiple conducting states and modulation by, for example, glycine (Johnson and Ascher, 1987) or Zn^{2+} (Peters et al., 1987; Westbrook and Mayer, 1987). Although careful tuning of the kinetic rate constants used to model AMPAR activation might reconcile this incongruity, it is beyond the scope of this paper.

Transmitter is temporarily trapped when bound to receptors. Thus, a large number of receptors, particularly high-affinity NMDARs, could increase the activation of AMPARs, not merely by slowing the clearance of transmitter from the cleft as a whole, but by retaining the transmitter very close to the AMPARs themselves. Such cooperativity among receptors would lead to a supralinear increase in their activation as a function of receptor number, and AMPAR activation would be greater when

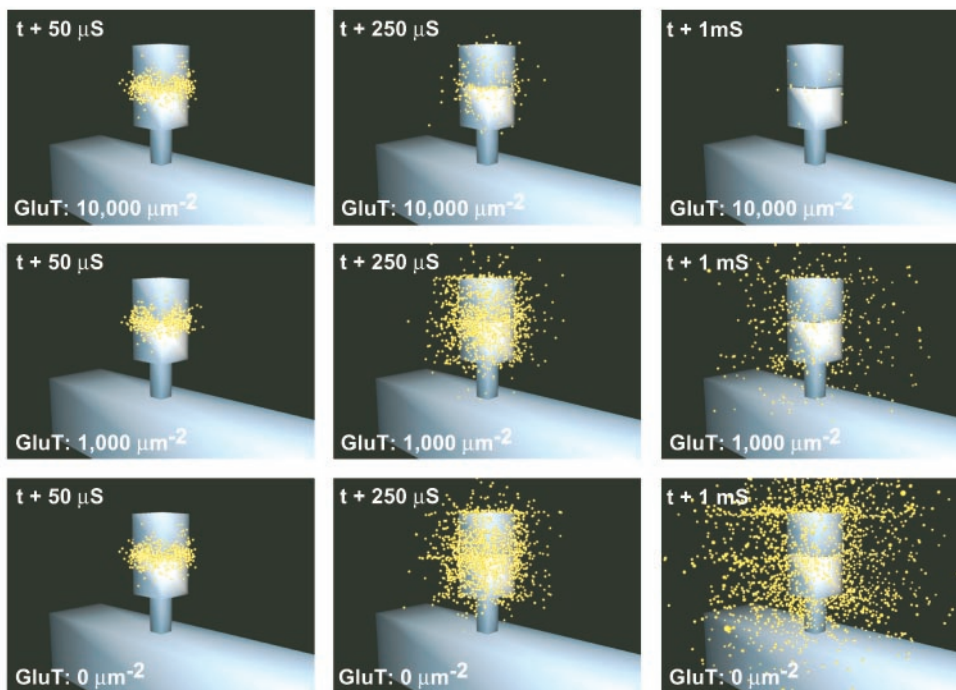


FIGURE 10 Glutamate spillout from the synaptic cleft. *Snapshots* of glutamate spillout as a function of time and glutamate transporter density (GluT). Individual glutamate molecules are shown as yellow spheres. The top cube represents the presynaptic bouton, separated from the spine by a 20 nm cleft. Transmitter was released as a point source in the center of the cleft at $t = 0$.

co-localized with a larger population of NMDARs. Instead, our simulations show that for physiological numbers of receptors, the number of open receptors scales directly with the total number of receptors, and the activation of individual receptors is independent of the other receptors at the synapse. This result further illustrates the power of the approach used here, as these subtle spatial interactions cannot be tested using analytic methods, and the number of spatial subdivisions required to accurately test this using a finite element model would be so large that the simulation would be computationally intractable (Bartol et al., 1991). Increasing quantal size also increased receptor activation, but because receptors became increasingly saturated, the size of the peak response was more sensitive to increases in n than increases in q . Thus, our results confirm that rapid insertion of AMPARs is an efficient way to increase synaptic efficacy. Increasing either the number of receptors at the synapse or quantal size also decreased quantal variability. Our simulations also predict that differences in the C.V.s of AMPA and NMDA-dependent EPSCs measured at a single synapse are due solely to differences in their total number.

Receptor saturation

We confirm that both AMPA and NMDA receptors are far from saturated after the instantaneous release of 3000 mol-

ecules of transmitter, and predict that saturation levels are almost completely dependent on the quantal size, regardless of the size of the receptor pool. This reflects the brief time course of glutamate in the synaptic cleft and the fact that a large fraction of the glutamate released from a vesicle diffused out of the cleft without ever binding synaptic receptors. Our simulations confirm that occupancy levels of AMPARs are similar to those of NMDARs (Holmes, 1995). This result may be unexpected because the higher affinity of NMDARs might suggest higher occupancy levels than for lower-affinity AMPARs. However, the difference in glutamate affinity of the two receptor types is due to differences in their glutamate dissociation rates; their forward binding rates are similar. When the decay of synaptic glutamate concentration from levels well above the EC_{50} of AMPARs to levels well below the EC_{50} of NMDARs is rapid, as was the case here, peak occupancy levels are largely determined by the rate at which receptors can bind transmitter rather than their overall affinity. When D_{Glu} was decreased and the clearance of transmitter from the cleft was slowed, saturation levels were governed by both association and dissociation rates (i.e., receptor affinity). Thus, although saturation levels for both AMPARs and NMDARs increase under conditions of slowed glutamate clearance, saturation of NMDARs becomes increasingly larger than AMPARs. Therefore, comparison of the relative saturation levels of AMPARs and NMDARs should allow independent de-

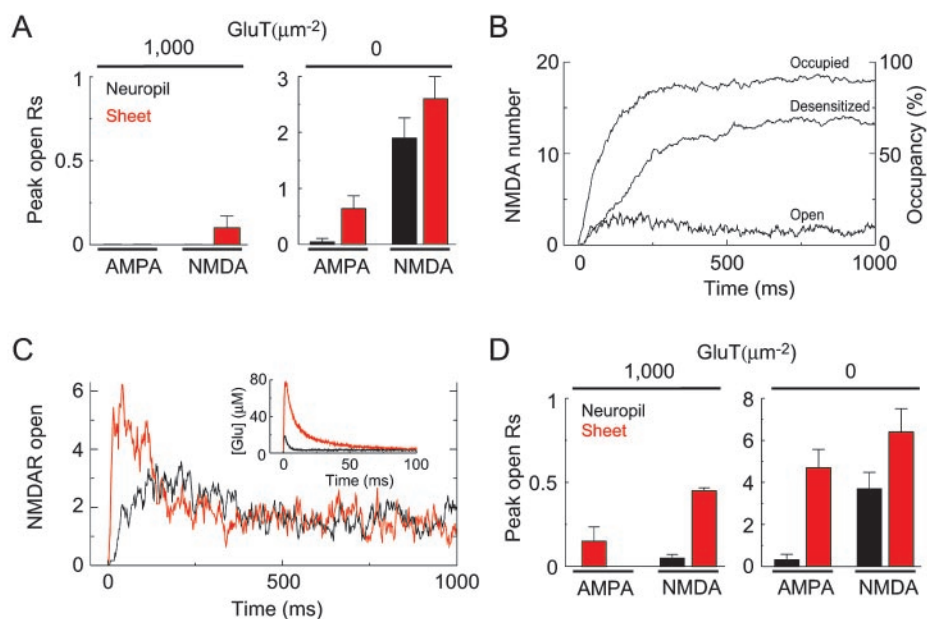


FIGURE 11 Glutamate spillover and extrasynaptic receptor activation. (A) Receptor activation following release of a single vesicle from a distant location in the neuropil or sheet. (B) Simultaneous release of four vesicles in the neuropil resulted in a low level of activation and a much higher level of receptor desensitization. (C) Differential activation of NMDARs in the neuropil (black trace) and sheet (red trace) following the simultaneous release of four quanta with glutamate uptake blocked. The inset shows the cleft glutamate concentration underlying this result. Note the tortuous neuropil dampens the spike in cleft glutamate caused by release at a neighboring site. Final resting [Glu] were similar in both conditions. (D) Summary of receptor activation following release of four quanta from neighboring sites in the neuropil and sheet. Data are given as mean \pm standard error ($n = 20$).

termination of the time course of synaptic glutamate concentration.

Comparison with earlier models

Previous models, including Monte Carlo (Faber et al., 1992; Wahl et al., 1996; Kruk et al., 1997) and finite element (Holmes, 1995; Kleinle et al., 1996) models of the time course of glutamate and receptor activation at simplified neuropils have been reported. Others give a highly idealized description of glutamate diffusion in which the neuropil is modeled as an isotropic porous medium (Rusakov and Kullmann, 1998; Barbour, 2001). The present approach is conceptually different from these because, unlike the former, the synapse is modeled in a spatially complex environment, and unlike the latter, the discreteness and inherent stochasticity of ligands, receptors, and their interactions were maintained. We were therefore able to address complex spatial interactions of transmitter and receptors within, and between, single synapses. Future modeling efforts to study glutamatergic synaptic transmission with MCell will utilize a 3-D reconstruction of hippocampal area CA1 neuropil obtained by high-resolution electron-microscope serial tomography (Frank, 1992); however, many of the features represented here for the canonical block geometry should hold in more realistic geometries.

CONCLUSIONS

We have presented a biophysically realistic model of activation of AMPA and NMDA receptors at a central glutamatergic synapse similar to the synapses made by Schaffer collateral fibers onto dendritic spines of pyramidal cells in the CA1 region of the hippocampus. The synaptic morphology described here also likely applies to many other synapses in the CNS, particularly in the cerebral cortex. Receptor activation and occupancy were both determined by the diffusion coefficient and number of molecules of glutamate released. Receptor activation, but not occupancy, was also sensitive to the size of the receptor pool. Activation of individual receptors was independent of other receptors co-localized at the same synapse, with physiological numbers of receptors. Therefore, a linear gain function describes the relation between receptor number and synaptic efficacy that can be directly adjusted by the rapid insertion and removal of receptors. The high density of uptake sites and the tortuosity of the neuropil prevented spillover, functionally isolating synapses. This independence between synapses maximizes storage capacity and permits sparse coding at individual synapses.

The authors thank Edwin Salpeter for valuable discussions, Jeffrey Isaacson, Esther Nimchinsky, Charles Stevens, Richard Weinberg, and Martina Wicklein for comments on the manuscript, and Vladan Lucic and Mary Kennedy for their continuing collaboration.

This work was supported by the Howard Hughes Medical Institute and the National Science Foundation.

K.M.F. and T.M.B., Jr. contributed equally to this project.

REFERENCES

- Andrasfalvy, B. K., and J. C. Magee. 2001. Distance-dependent increase in AMPA receptor number in the dendrites of adult hippocampal CA1 pyramidal neuron. *J. Neurosci.* 21:9151–9159.
- Arriza, J. L., W. A. Fairman, J. I. Wadiche, G. H. Murdoch, M. P. Kavanaugh, and S. G. Amara. 1994. Functional comparisons of three glutamate transporter subtypes cloned from human motor cortex. *J. Neurosci.* 14:5559–5569.
- Auger, C., and D. Attwell. 2000. Fast removal of synaptic glutamate by postsynaptic transporters. *Neuron.* 28:547–558.
- Barbour, B. 2001. An evaluation of synapse independence. *J. Neurosci.* 21:7969–7984.
- Barbour, B., H. Brew, and D. Attwell. 1991. Electrogenic uptake of glutamate and aspartate into glial cells isolated from the salamander (*Ambystoma*) retina. *J. Physiol. (Lond.)* 436:169–193.
- Bartol, Jr., T. M. 1992. A study of miniature endplate current generation at the vertebrate neuromuscular junction using electrophysiology and Monte Carlo simulation. Ph.D. thesis, Cornell University, Ithaca, N
- Bartol, Jr., T. M., B. R. Land, E. E. Salpeter, and M. M. Salpeter. 1991. Monte Carlo simulation of miniature endplate current generation in the vertebrate neuromuscular junction. *J. Biophys.* 59:1290–1307.
- Bekkers, J. M., and C. F. Stevens. 1989. NMDA and non-NMDA receptors are co-localized at individual excitatory synapses in cultured rat hippocampus. *Nature.* 341:230–233.
- Bergles, D. E., J. A. Dzuby, and C. E. Jahr. 1997. Glutamate transporter currents in Bergmann glial cells follow the time course of extrasynaptic glutamate. *Proc. Natl. Acad. Sci. USA.* 94:14821–14825.
- Carroll, R. C., D. V. Lissin, M. von Zastrow, R. A. Nicoll, and R. C. Malenka. 1999. Rapid redistribution of glutamate receptors contributes to long-term depression in hippocampal cultures. *Nat. Neurosci.* 2:454–460.
- Chaudhry, F. A., K. P. Lehre, M. van Lookeren Campagne, O. P. Ottersen, N. C. Danbolt, and J. Storm-Mathisen. 1995. Glutamate transporters in glial plasma membranes: highly differentiated localizations revealed by quantitative ultrastructural immunocytochemistry. *Neuron.* 15:711–720.
- Chen, K. C., and C. Nicholson. 2000. Changes in brain cell shape create residual extracellular space volume and explain tortuosity behavior during osmotic challenge. *Proc. Natl. Acad. Sci. USA.* 97:8306–8311.
- Clements, J. D. 1996. Transmitter timecourse in the synaptic cleft: its role in central synaptic function. *TINS.* 19:163–171.
- Clements, J. D., R. A. Lester, G. Tong, C. E. Jahr, and G. L. Westbrook. 1992. The time course of glutamate in the synaptic cleft. *Science.* 258:1498–1501.
- Danbolt, N. C., F. A. Chaudhry, Y. Dehnes, K. P. Lehre, L. M. Levy, K. Ullensvang, and J. Storm-Mathisen. 1998. Properties and localization of glutamate transporters. *Prog. Brain Res.* 116:23–43.
- Diamond, J. S. 2001. Neuronal glutamate transporters limit activation of NMDA receptors by neurotransmitter spillover on CA1 pyramidal cells. *J. Neurosci.* 21:8328–8338.
- Diamond, J. S., and C. E. Jahr. 1997. Transporters buffer synaptically released glutamate on a submillisecond time scale. *J. Neurosci.* 17:4672–4687.
- Eccles, J. C., and J. C. Jaeger. 1958. The relationship between the mode of operation and the dimensions of the junctional regions at synapses and motor end-organs. *Proc. R. Soc. Lond. (Biol.)* 148:38–56.
- Eccles, J. C., B. Katz, and S. W. Kuffler. 1942. Effects of eserine on neuromuscular transmission. *J. Neurophys.* 5:211–230.
- Ellis, R. J. 2001. Macromolecular crowding: obvious but underappreciated. *TIBS.* 26:597–604.
- Elowitz, M. B., M. G. Surette, P. E. Wolf, J. B. Stock, and S. Leibler. 1999. Protein mobility in the cytoplasm of *Escherichia coli*. *J. Bacteriol.* 181:197–203.
- Faber, D. S., W. S. Young, P. Legendre, and H. Korn. 1992. Intrinsic quantal variability due to stochastic properties of receptor-transmitter interactions. *Science.* 258:1494–1498.
- Ferkany, J., and J. T. Coyle. 1986. Heterogeneity of sodium-dependent excitatory amino acid uptake mechanisms in rat brain. *J. Neurosci. Res.* 16:491–503.
- Frank, J. 1992. Electron Tomography: Three-Dimensional Imaging with the TEM. Plenum, New York.
- Frerking, M., and M. Wilson. 1996. Saturation of postsynaptic receptors at central synapses? *Curr. Opin. Neurobiol.* 6:395–403.
- Geiger, J. R. P., A. Roth, B. Tasskin, and P. Jonas. 1999. Glutamate-mediated synaptic excitation of cortical interneurons. In *The Handbook of Experimental Pharmacology*, Vol. 141. Retinoids, Ionotropic Glutamate Receptors in the CNS. P. Jonas and H. Monyer, editors. Springer-Verlag, Berlin.
- Harris, K. M., and S. B. Kater. 1994. Dendritic spines: cellular specializations imparting both stability and flexibility to synaptic function. *Annu. Rev. Neurosci.* 17:341–371.
- Hayashi, Y., S. H. Shi, J. Esteban, A. Piccini, J. C. Poncer, and R. Malinow. 2000. Driving AMPA receptors into synapses by LTP and CaMKII: requirement for GluR1 and PDZ domain interaction. *Science.* 287:2262–2267.
- Hestrin, S., P. Sah, and R. A. Nicoll. 1990. Mechanisms generating the time course of dual component excitatory synaptic currents recorded in hippocampal slices. *Neuron.* 5:247–253.
- Hjelmstad, G. O., J. T. Isaac, R. A. Nicoll, and R. Malenka. 1997. Lack of AMPA receptor desensitization during basal synaptic transmission in the hippocampal slice. *J. Neurophys.* 81:3096–3099.
- Holmes, W. R. 1995. Modeling the effect of glutamate diffusion and uptake on NMDA and non-NMDA receptor saturation. *Biophys. J.* 69:1734–1747.
- Isaac, J. T., R. A. Nicoll, and R. C. Malenka. 1995. Evidence for silent synapses: implications for the expression of LTP. *Neuron.* 15:427–434.
- Isaacson, J. S., and R. A. Nicoll. 1993. The uptake inhibitor *L-trans*-PDC enhances responses to glutamate but fails to alter the kinetics of excitatory synaptic currents in the hippocampus. *J. Neurophys.* 70:187–191.
- Johnson, J. W., and P. Ascher. 1987. Glycine potentiates the nmda response in cultured mouse brain neurons. *Nature.* 325:529–531.
- Jonas, P., G. Major, and B. Sakmann. 1993. Quantal components of unitary EPSCs at the mossy fibre synapse on CA3 pyramidal cells of rat hippocampus. *J. Physiol. (Lond.)* 472:615–663.
- Kharazia, V. N., K. D. Phend, A. Rustioni, and R. J. Weinberg. 1996. EM colocalization of AMPA and NMDA receptor subunits at synapses in rat cerebral cortex. *Neurosci. Lett.* 210:37–40.
- Kharazia, V. N., and R. J. Weinberg. 1997. Tangential synaptic distribution of NMDA and AMPA receptors in rat neocortex. *Neurosci. Lett.* 238:41–44.
- Kharazia, V. N., and R. J. Weinberg. 1999. Immunogold localization of AMPA and NMDA receptors in somatic sensory cortex of albino rat. *J. Comp. Neurol.* 412:292–302.
- Kleinle, J., K. Vogt, H. R. Luscher, L. Muller, W. Senn, J. Wyler, and K. Streit. 1996. Transmitter concentration profiles in the synaptic cleft: an analytical model of release and diffusion. *Biophys. J.* 71:2413–2426.
- Kruk, P. J., H. Korn, and D. S. Faber. 1997. The effects of geometrical parameters on synaptic transmission: a Monte Carlo simulation study. *Biophys. J.* 73:2874–2890.
- Lehre, K. P., and N. C. Danbolt. 1998. The number of glutamate transporter subtype molecules at glutamatergic synapses: chemical and stereological quantification in young adult rat brain. *J. Neurosci.* 18:8751–8757.
- Lester, R. A., J. D. Clements, G. L. Westbrook, and C. E. Jahr. 1990. Channel kinetics determine the time course of NMDA receptor-mediated synaptic currents. *Nature.* 346:565–567.
- Lester, R. A., and C. E. Jahr. 1992. NMDA channel behavior depends on agonist affinity. *J. Neurosci.* 12:635–643.

- Levy, L. M., O. Warr, and D. Attwell. 1998. Stoichiometry of the glial glutamate transporter GLT-1 expressed inducibly in a Chinese hamster ovary cell line selected for low endogenous Na⁺-dependent glutamate uptake. *J. Neurosci.* 18:9620–9628.
- Liao, D., N. A. Hessler, and R. Malinow. 1995. Activation of postsynaptically silent synapses during pairing-induced LTP in CA1 region of hippocampal slice. *Nature.* 375:400–404.
- Liu, G., S. Choi, and R. W. Tsien. 1999. Variability of neurotransmitter concentration and nonsaturation of postsynaptic AMPA receptors at synapses in hippocampal cultures and slices. *Neuron.* 22:395–409.
- Longworth, L. G. 1953. Diffusion measurements at 25°C, of aqueous solutions of amino acids, peptides and sugars. *J. Am. Chem. Soc.* 75:5705–5709.
- Magee, J. C., and E. P. Cook. 2000. Somatic EPSP amplitude is independent of synapse location in hippocampal pyramidal neurons. *Nat. Neurosci.* 3:895–903.
- Mainen, Z. F., R. Malinow, and K. Svoboda. 1999. Synaptic calcium transients in single spines indicate that NMDA receptors are not saturated. *Nature.* 399:151–155.
- Matsubara, A., J. H. Laake, S. Davanger, S. Usami, and O. P. Ottersen. 1996. Organization of AMPA receptor subunits at a glutamate synapse: a quantitative immunogold analysis of hair cell synapses in the rat organ of Corti. *J. Neurosci.* 16:4457–4467.
- Matsuzaki, M., G. C. Ellis-Davies, T. Nemoto, Y. Miyashita, M. Iino, and H. Kasai. 2001. Dendritic spine geometry is critical for AMPA receptor expression in hippocampal CA1 pyramidal neurons. *Nat. Neurosci.* 4:1086–1092.
- McAllister, A. K., and C. F. Stevens. 2000. Nonsaturation of AMPA and NMDA receptors at hippocampal synapses. *Proc. Natl. Acad. Sci. USA.* 97:6173–6178.
- Nusser, Z., R. Lujan, G. Laube, J. Roberts, E. Molnar, and P. Somogyi. 1998. Cell type and pathway dependence of synaptic AMPA receptor number and variability in the hippocampus. *Neuron.* 21:545–559.
- Nusser, Z., E. Mulvihill, P. Streit, and P. Somogyi. 1994. Subsynaptic segregation of metabotropic and ionotropic glutamate receptors as revealed by immunogold localization. *Neuroscience.* 61:421–427.
- Otis, T. S., and C. E. Jahr. 1998. Anion currents and predicted glutamate flux through a neuronal glutamate transporter. *J. Neurosci.* 15:7099–7110.
- Patneau, D. K., and M. L. Mayer. 1990. Structure-activity relationships for amino acid transmitter candidates acting at *N*-methyl-D-aspartate and quisqualate receptors. *J. Neurosci.* 10:2385–2399.
- Peters, S., J. Koh, and D. W. Choi. 1987. Zinc selectively blocks the action of *N*-methyl-D-aspartate on cortical neurons. *Science.* 236:589–593.
- Racca, C., F. A. Stephenson, P. Streit, J. Roberts, and P. Somogyi. 2000. NMDA receptor content of synapses in stratum radiatum of the hippocampal CA1 area. *J. Neurosci.* 20:2512–2522.
- Rothstein, J. D., L. Martin, A. I. Levey, M. Dykes-Hoberg, L. Jin, D. Wu, N. Nash, and R. W. Kuncl. 1994. Localization of neuronal and glial glutamate transporters. *Neuron.* 13:713–725.
- Rusakov, D. A., and D. M. Kullmann. 1998. Extrasynaptic glutamate diffusion in the hippocampus: ultrastructural constraints, uptake, and receptor activation. *J. Neurosci.* 18:3158–3170.
- Sarantis, M., L. Ballerini, B. Miller, R. A. Silver, M. Edwards, and D. Attwell. 1993. Glutamate uptake from the synaptic cleft does not shape the decay of the non-NMDA component of the synaptic current. *Neuron.* 11:541–549.
- Shi, S. H., Y. Hayashi, R. S. Petralia, S. H. Zaman, R. J. Wenthold, K. Svoboda, and R. Malinow. 1999. Rapid spine delivery and redistribution of AMPA receptors after synaptic NMDA receptor activation. *Science.* 284:1811–1816.
- Spruston, N., P. Jonas, and B. Sakmann. 1995. Dendritic glutamate receptor channels in rat hippocampal CA3 and CA1 pyramidal neurons. *J. Physiol. (Lond.).* 482(Pt 2):325–352.
- Stevens, C. F., and Y. Wang. 1995. Facilitation and depression at single central synapses. *Neuron.* 14:795–802.
- Stiles, J. R., and T. M. Bartol, Jr. 2001. Monte Carlo methods for simulating realistic synaptic microphysiology. In *Computational Neuroscience Realistic Modeling for Experimentalists*, E. de Schutter, editor. CRC press, Boca Raton, FL. 681–731.
- Stiles, J. S., T. M. Bartol, Jr., M. M. Salpeter, E. E. Salpeter, and T. J. Sejnowski. 2001. Synaptic variability: new insights from reconstructions and Monte Carlo simulations with MCell. In *Synapses* W. M. Cowan, T. C. Sudhof, and C. F. Stevens, editors. Johns Hopkins University Press, Baltimore, MD. 87–128.
- Stiles, J. R., D. van Helden, T. M. Bartol, Jr., E. E. Salpeter, and M. M. Salpeter. 1996. Miniature endplate current rise times less than 100 microseconds from improved dual recordings can be modeled with passive acetylcholine diffusion from a synaptic vesicle. *Proc. Natl. Acad. Sci. USA.* 93:5747–5752.
- Takumi, Y., V. Ramirez-Leon, P. Laake, E. Rinivik, and O. P. Ottersen. 1999. Different modes of expression of AMPA and NMDA receptors in hippocampal synapses. *Nat. Neurosci.* 2:618–624.
- Tong, G., and C. E. Jahr. 1994. Block of glutamate transporters potentiates postsynaptic excitation. *Neuron.* 13:1195–1203.
- Valtschanoff, J. G., A. Burette, R. J. Wenthold, and R. J. Weinberg. 1999. Expression of nr2 receptor subunit in rat somatic sensory cortex: synaptic distribution and colocalization with NR1 and PSD-95. *J. Comp. Neurol.* 410:599–611.
- Ventura, R., and K. M. Harris. 1999. Three-dimensional relationships between hippocampal synapses and astrocytes. *J. Neurosci.* 19:6897–6906.
- Wadiche, J. I., J. L. Arriza, S. G. Amara, and M. P. Kavanaugh. 1995. Kinetics of a human glutamate transporter. *Neuron.* 14:1019–1027.
- Wahl, L. M., C. Pouzat, and K. J. Stratford. 1996. Monte Carlo simulation of fast excitatory synaptic transmission at a hippocampal synapse. *J. Neurophys.* 75:597–608.
- Westbrook, G. L., and M. L. Mayer. 1987. Micromolar concentrations of Zn²⁺ antagonize NMDA and GABA responses of hippocampal neurons. *Nature.* 328:640–643.
- Williams, S. R., and G. J. Stuart. 2002. Dependence of EPSP efficacy on synapse location in neocortical pyramidal neurons. *Science.* 295:1907–1910.
- Wu, G., R. Malinow, and H. T. Cline. 1996. Maturation of a central glutamatergic synapse. *Science.* 274:972–976.
- Zerangue, N., and M. P. Kavanaugh. 1996. Flux coupling in a neuronal glutamate transporter. *Nature.* 383:634–637.